ELSEVIER

Polymer 40 (1999) 2151–2162

polymer

Characterization of chemical structure and morphology of eroding polyanhydride copolymers by liquid-state and solid-state ^{1}H n.m.r.

David L. McCann[a], Frank Heatley[b,*], Antony D'Emanuele[c]

[a]*Abbott Laboratories Ltd, Queenborough, Kent ME11 5EL, UK*
[b]*Department of Chemistry, University of Manchester, Manchester M13 9PL, UK*
[c]*School of Pharmacy and Pharmaceutical Sciences, University of Manchester, Manchester M13 9PL, UK*

Received 6 April 1998; accepted 22 May 1998

Abstract

An n.m.r. investigation of the chemical and morphological changes occurring during erosion in pH 7.4 phosphate buffer at 37°C of melt-fabricated polyanhydride devices formed from copolymers of 1,3-bis(*p*-carboxyphenoxy)propane (CPP) and sebacic acid (SA) is reported. From sequence distributions determined using solution-state ^{1}H n.m.r. spectroscopy, the following order of anhydride bond lability was determined: SA–SA ≈ SA–CPP ≫ CPP–CPP, leading to preferential hydrolysis of aliphatic blocks within the copolymer chain. Solid-state ^{1}H and ^{2}H n.m.r. spectroscopy were used to investigate morphological changes occurring during erosion. Both indicated significant absorption of mobile water after *ca*. 10 h. Subtle variations in the symmetry of the narrow signals confirmed the changes in chemical composition apparent from high resolution ^{1}H n.m.r. analysis. In the initial stages, there was an increase in crystallinity attributed to preferential erosion of amorphous regions.

Keywords: Erosion; Polyanhydride copolymers; ^{1}H n.m.r. analysis

1. Introduction

Polyanhydride copolymers of 1,3-bis(*p*-carboxyphenoxy) propane (CPP) and sebacic acid (SA), p(CPP–SA), have been extensively used in the preparation of biodegradable implants for a variety of drug delivery applications. Much of the interest in this class of biomaterials has stemmed from the apparent surface-eroding characteristics initially noted in some copolymers, which are uniquely achieved without the inclusion of potentially allergenic matrix additives [1]. Recognition of the importance of erosion in controlling drug release from these materials has driven much recent research activity towards achieving a more thorough understanding of the erosion process. Morphological characterization of eroding polyanhydride devices has been performed with the aid of scanning electron microscopy [2], light microscopy [3], and most recently in situ atomic force microscopy [4] and magnetic resonance imaging [5]. Göpferich and Langer [6] have examined the influence of polymer microstructure and monomer solubility on the erosion process and proposed a model to predict porosity and mass balance changes occurring within eroding matrices [7]. With regard to detailed chemical analysis of polyanhydride erosion, despite the established use of high resolution ^{1}H n.m.r. for the characterization of patent polymers [8,9], the principal studies on eroded specimens performed to date have relied upon vibrational spectroscopy using direct [3] and indirect Raman [10] measurements. With both techniques, characteristic anhydride carbonyl bands are clearly discernible during polymer erosion as is the emergence of the complementary carbonyl band associated with the formation of carboxylic acid end groups. Raman spectroscopy is also sensitive to increases in C-C deformation which accompany enhanced methylene chain mobility in the low molecular weight oligomeric degradation products. However, given the complexity of the polyanhydride erosion process and the absence of suitable reference standards, vibrational spectroscopy cannot match the quantitative insight into chain structure afforded by n.m.r.

The sensitivity of n.m.r. to short range atomic interactions also provides a means of investigating the molecular dynamics of polymers in the solid-state. The advantage of such measurements is that information relating to motional heterogeneity, which often underpins the macroscopic physical properties of the polymer, can be readily obtained

* Corresponding author.

0032-3861/99/$ - see front matter
PII: S0032-3861(98)00434-0

without the need for sophisticated and/or destructive sample preparation techniques. Comprehensive reviews of the application of solid-state n.m.r. spectroscopy in polymer science have been provided by a number of workers [11–13]. N.m.r has proved to be particularly informative for investigating the behaviour of water within solids since it can provide an insight into the molecular mobilities of both absorbed water and the solid-substrate as a function of water content. The utility of such analysis has been demonstrated for hydrated poly(vinylpyrrolidone) [14], cationically charged poly(vinyl alcohol) gel matrices [15] and poly(2-hydroxyethylmethacrylate) hydrogels [16]. ^{2}H n.m.r., in particular, has seen widespread use as a selective probe of water mobility within hydrated solids. In the absence of chemical exchange, the relaxation times characterizing the ^{2}H n.m.r. lineshape specifically reflect the relative mobilities of water molecules present within the specimen. Poly(*N*-vinyl-2-pyrrolidone-*co*-methyl methacrylate) hydrogels [17], low density poly(ethylene)s [18] and poly(D,L-lactide-*co*-glycolide) [19] are among the polymeric materials studied by this technique.

This paper reports an investigation of the chemical and morphological changes occurring during erosion of p(CPP–SA) by pH 7.4 phosphate buffer. The copolymer composition and comonomer dyad sequence distributions were determined using liquid-state ^{1}H n.m.r. spectroscopy, while wideline solid-state ^{1}H and ^{2}H n.m.r. was employed to monitor morphological changes in the eroding matrices.

2. Experimental section

2.1. Polymer synthesis and characterization

p(CPP–SA) copolymers with CPP–SA molar ratios 12.5:87.5 and 30:70 were synthesized by melt-polycondensation of mixed anhydrides of diacids and acetic acid as previously described [20]. The composition and sequence distributions were determined by ^{1}H n.m.r. [8]. Samples were dissolved in chloroform-d_1 (99.8% atom-*d*) and chemical shifts were referenced to tetramethylsilane (99.9%) (Goss Scientific, Glossop, UK). Polymer molecular weights were determined relative to poly(styrene) standards (580–860 000; Polymer Laboratories Ltd, Church Stretton, UK and Pressure Chemical Company, Pittsburgh, USA) by size exclusion chromatography (SEC). Samples were eluted in ethanol-free chloroform through a PLgel 5 μm mixed-D 0.75 $\times$ 30 cm column (Polymer Laboratories Ltd.) at a flow rate of 1 cm^3 min^{-1} at 25°C prior to detection by a differential refractometer (Waters Associates Model 410, Millipore Ltd, Watford, UK). Toluene at a concentration of 0.35% v/v was used as a flow-rate marker in both standards and samples. Chromatograms were analysed using Millennium 2010 v2.00 system software (Waters Associates).

2.2. Device Fabrication

Disks of mass 100 $\pm$ 1 mg and size 10.4 mm diameter and ~1.1 mm thickness were prepared by melt-compression in PTFE moulds [21]. Polymers were milled under liquid nitrogen (Polymix Model A10 Analytical Mill, Kinematica, Switzerland), sieved to $<$ 355 μm and lyophilized at 0.1 mbar over di-phosphorus pentaoxide (Modulo Freeze Dryer, Edwards High Vacuum International, Crawley, UK) before use. After precompression at 25°C, the polymers were compressed at 80°C using a hydraulic press (Beckmann Instruments Ltd, High Wycombe, UK). Devices were allowed to cool to 25°C in a dessicator and then stored in foil pouches under dry nitrogen over di-phosphorus pentaoxide at −80°C.

2.3. In vitro erosion

p(CPP–SA) disks with initial weight-average molecular masses of ~20 000 were eroded in either: (1) pH 7.4 phosphate buffer USP; or (2) deuterated pH 7.4 phosphate buffer USP under gentle agitation at 37°C (Model SI50 incubator shaker, Stuart Scientific, Lutterworth, UK). Deuterated buffer was prepared using 25:75% v/v D_2O–H_2O (D_2O, 99.9% atom-*d*, Goss Scientific, Glossop, UK). Buffer solutions were changed periodically to maintain sink conditions throughout device erosion. At intervals, disks were removed, rinsed with H_2O or D_2O–H_2O as appropriate to remove adherent buffer, and gently blotted to remove surface water. The disks were then frozen in liquid nitrogen, lyophilized for 24 h at 0.1 mbar over di-phosphorus pentaoxide and stored under dry nitrogen over di-phosphorus pentaoxide at − 80°C.

2.4. Water absorption by gravimetry.

Eroded samples were dried to constant weight under vacuum (0.1 mbar) over di-phosphorus pentaoxide and anhydrous silica gel. Water and D_2O–H_2O contents were determined from the mass difference between the wet and dry states, and the weight loss from eroded disks was determined from the mass difference between the original and eroded dry states. H_2O absorption measurements were performed in duplicate but D_2O–H_2O absorption values were single determinations.

2.5. High resolution ^{1}H n.m.r. spectroscopy

Following gentle blotting to remove surface water, samples of eroded polymer were dissolved in tetrahydrofuran-d_8 (THF-d_8, 99.6% atom-*d*, Fluorochem Ltd., Glossop, UK) at a concentration of 0.5% w/w. ^{1}H n.m.r. spectra were immediately recorded at 25°C using a Jeol JNM-EX270 spectrometer operating at 270 MHz. The spectrum of the uneroded polymer was obtained at the same concentration using $CDCl_3$ (99.8% atom-*d*, Fluorochem Ltd, Glossop, UK) as solvent. A

45° flip angle pulse was used with a 4 s pulse delay to ensure complete relaxation at the end of each cycle, and 32 K data points were acquired. Chemical shifts were referenced to the residual proton signal at 2.6 ppm in THF-d_8 or 7.25 ppm in $CDCl_3$.

2.6. Solid-state ^1H n.m.r. spectroscopy

Eroded polymer disks were gently blotted to remove surface water and packed into short 5 mm o.d. n.m.r. tubes, ensuring as far as possible that the masses and volume occupied were the same for all samples. Solid-state ^1H n.m.r. spectra were recorded at 25°C, immediately after sample preparation, using a Varian Associates Unity 300 spectrometer operating at 300 MHz. A Doty Scientific 5 mm ^1H CRAMPS probe was used though magic-angle spinning was not employed. Spectra were obtained by Fourier transformation of the free induction decay following 90° pulses of width 1.5 μs using a spectral width of 500 kHz, a probe recovery delay of 5 μs and a pulse interval of 20 s sufficient to allow full relaxation.

2.7. Solid-State ^2H n.m.r. spectroscopy

The same samples and spectrometer as for solid-state ^1H n.m.r. were used operating at 46 MHz. A Doty Scientific 7 mm magic-angle spinning probe was used though again magic-angle spinning was not employed. Spectra were obtained by Fourier transformation of the free induction decay following 90° pulses of width ? μs using a spectral width of 25 kHz, a probe recovery delay of 5 μs and a pulse interval of 20 s, sufficient to allow full relaxation.

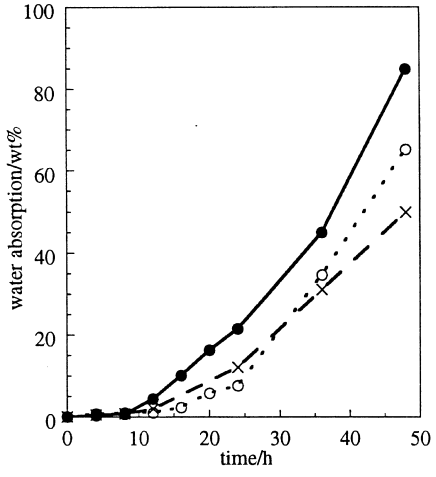

Fig. 1. Water absorption (wt.%) in p(CPP–SA) 12.5:87.5 and p(CPP–SA) 30:70 devices during erosion in pH 7.4 phosphate buffer USP. ●, p(CPP–SA) 12.5:87.5 in H_2O; ○, p(CPP–SA) 12.5:87.5 in 25:75 D_2O–H_2O; ×, p(CPP–SA) 30:70 in H_2O.

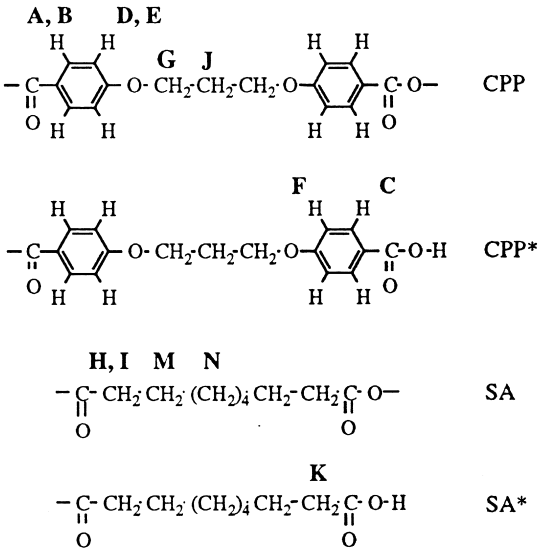

Scheme 1.

3. Results and discussion

3.1. Water absorption by gravimetry.

Fig. 1 shows water absorption as a function of erosion time for samples exposed to H_2O and 25:75 D_2O–H_2O buffers. Although the D_2O–H_2O absorption was somewhat lower than that of H_2O, possibly due to an isotope effect, both curves show an induction period of ca. 10 h during

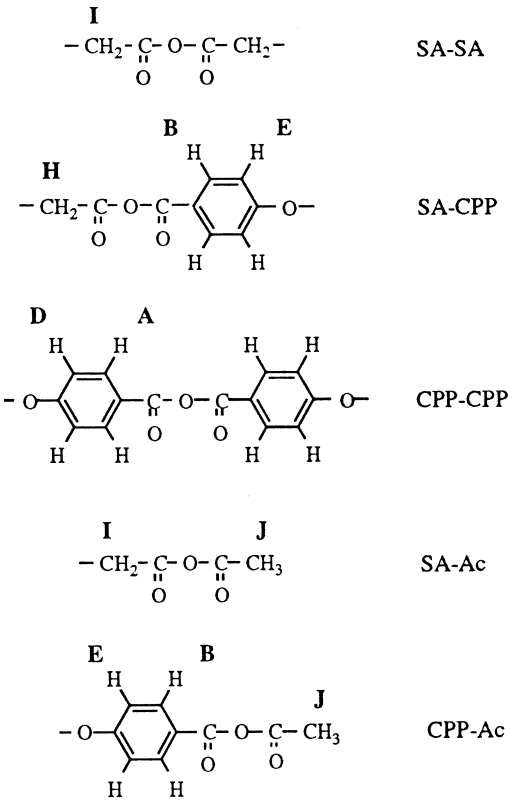

Scheme 2.

which the water absorption is very low, followed by increasingly rapid absorption.

3.2. High resolution ^1H n.m.r.

As p(CPP–SA) copolymers have been shown to be susceptible to depolymerization in solution [22], spectra were acquired immediately after dissolution to minimize the impact of chain scission. THF-d_8 proved to be a suitable solvent for p(CPP–SA) 12.5:87.5 and its degradation products over the timescale of the current study but solubility constraints at higher CPP contents prevented use of the technique for the analysis of p(CPP–SA) 30:70 devices.

Structural units and nucleus labelling relevant to the n.m.r. analysis are shown in Schemes 1 and 2.

Fig. 2 compares the ^{1}H n.m.r. spectra of p(CPP–SA) 12.5:87.5 devices before erosion and after 24 h erosion. There was a slight difference in chemical shifts between corresponding peaks in the two spectra attributable to the use of different solvents.

Considering first the low frequency region, the triplets H and I at 2.60 and 2.44 ppm ($J = 7.3$ Hz) were assigned to SA–CPP and SA–SA dyads, respectively [8], while the singlet L at 2.17 ppm was assigned to methyl groups on acetyl residues (Ac) at the chain ends and/or the methyl groups of acetic anhydride, a potential impurity. During device erosion there were notable reductions in the intensities of peaks I and L. In the case of peak L, this change was brought about by hydrolysis of acetyl end groups and acetic anhydride impurity by absorbed water. The acetic acid formed in both reactions was progressively leached out of the polymer matrix into the aqueous medium, and therefore made a diminishing contribution to the spectra of the eroded specimens. Decreases in the intensity of peak I were brought

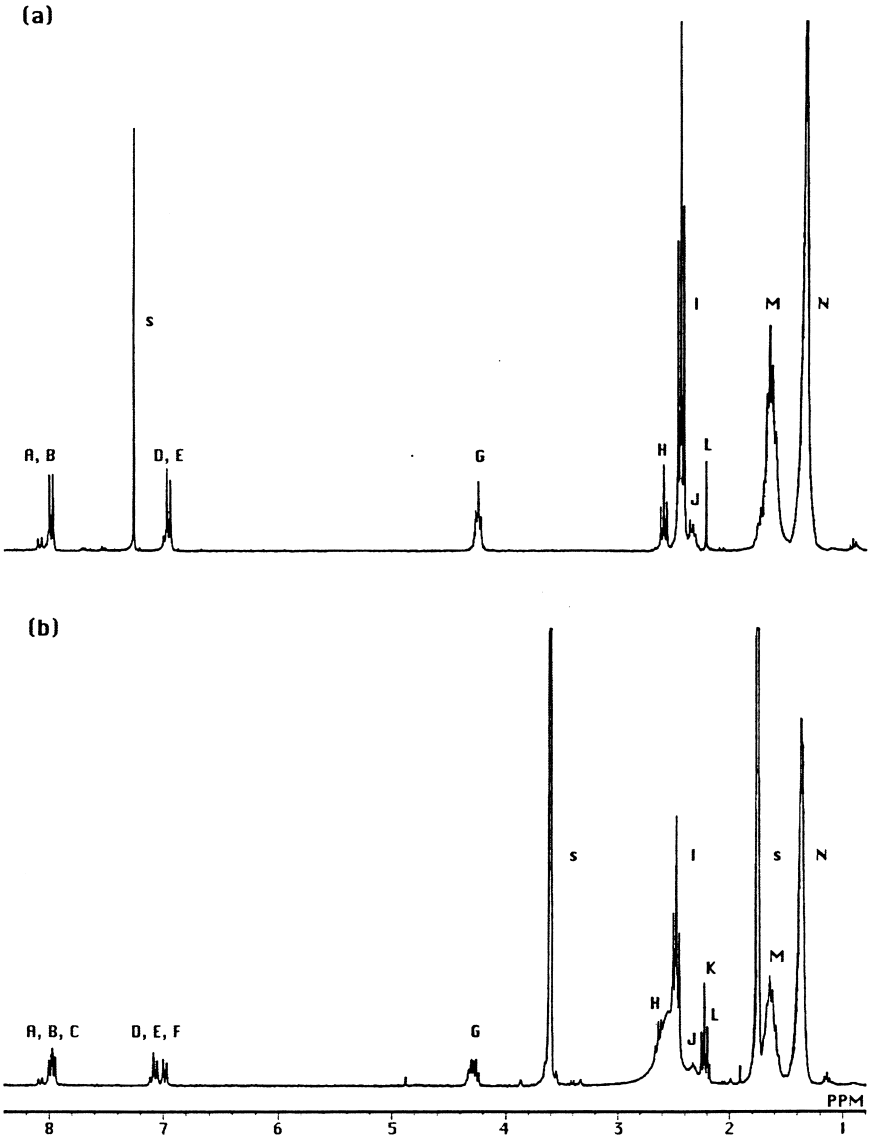

Fig. 2. ^{1}H n.m.r. spectra of p(CPP–SA) 12.5:87.5. (a) uneroded polymer run in $CDCl_3$; (b) eroded for 24 h in pH 7.4 phosphate buffer USP, run in THF-d_8. The label *s* indicates residual solvent proton resonances.

about by scission of SA–SA links in the polymer. These changes were accompanied by the emergence of a new triplet K at 2.22 ppm ($J = 7.3$ Hz) attributed to SA end groups, designated SA*.

A low frequency signal not present in the uneroded polymer, but which made an increasingly important contribution to the spectra of eroded devices, particularly between 12 and 48 h, was a broad resonance at ca. 2.6 ppm. This signal was attributed to absorbed water. The increase in intensity of this peak broadly replicated the extent of water absorption as measured by gravimetry (Fig. 1). After 48 h erosion, when the extent of water absorption reaches ~80% w/w, this peak completely subsumed peak K while at the same time dominating peak I.

The high frequency (aromatic) region is shown as a function of erosion time in Fig. 3. The observed doublets are labelled in the spectrum of the 24 h eroded sample.

The spectrum of the uneroded polymer clearly showed two intense doublets B and E at 7.99 and 7.07 ppm ($J = 8.9$ Hz) assigned [8] to aromatic protons in CPP–CPP dyads as indicated in Schemes 1 and 2. The small peak appearing at 7.01 ppm was interpreted as the high frequency component of a doublet D centred at 6.99 ppm, the low frequency component of which was obscured by the high frequency component of doublet E; this doublet, together with a weaker doublet A at 8.08 ppm ($J = 8.9$ Hz), was assigned to CPP–SA dyads as indicated in Schemes 1 and 2. These principal resonances appeared in the spectra of the eroded devices. Within 4 h erosion, two new signals emerged, a doublet F at 6.99 ppm ($J = 8.9$ Hz) and a peak formed on the low frequency component of doublet B at ca. 7.95 ppm. Changes in the symmetry of peak B between 4 and 24 h suggest that this latter peak is actually the low frequency component of a doublet C at 7.97 ppm ($J = 8.9$ Hz), whose high frequency component is obscured by the low frequency component of peak B. During erosion, the intensities of the new doublets at 6.99 and 7.97 ppm grew in parallel, mirrored by a decrease in the intensity of the original polymer dyad resonances. The new signals were attributed to CPP end groups, designated CPP*, as indicated in Schemes 1 and 2. The CPP* units are formed during erosion by hydrolysis of the CPP-SA and CPP-CPP links. The fact that the CPP* resonances appear to low frequency of CPP moieties in the backbone is consistent with the higher electron density around the contributing protons (shielding effect) which arises as a result of the reduced electronegativity of the COOH end group compared to the anhydride link in the polymer chain.

3.3. Polymer composition and sequence distribution

Having identified the principal ^{1}H n.m.r. spectral components, the structural characterization of the eroding polymer was performed on the basis of the following statistical parameters.

3.3.1. Monomer fractions

Monomer fractions, (SA) and (CPP) (i.e. mole fraction of SA and CPP), were determined from the relative intensities of the peaks at 1.3 ppm (SA units, eight protons) and 6.9–8.1 ppm (CPP units, eight protons).

3.3.2. Dyad and end-group fractions

The polymer chain may be represented by the following dyads and end-groups (Schemes 1 and 2):

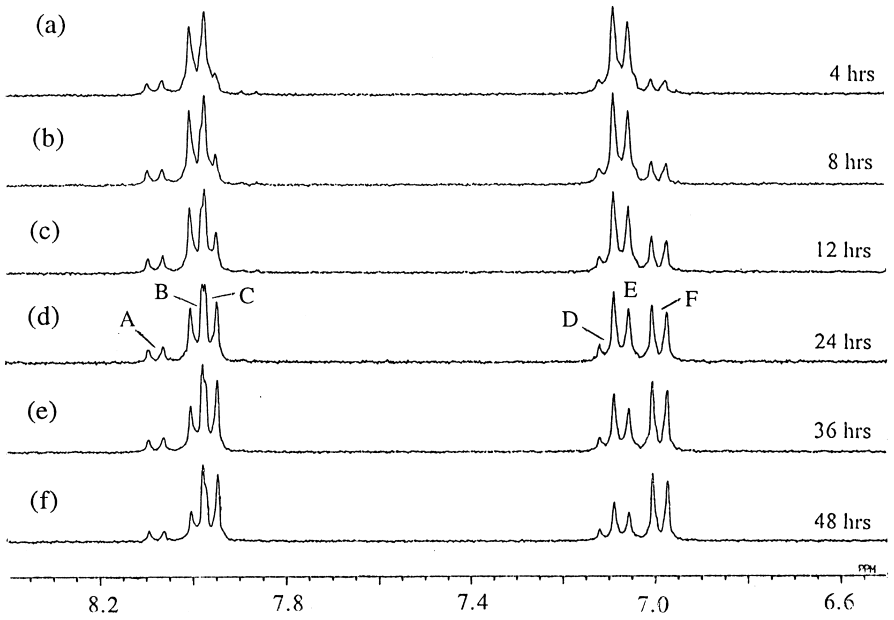

Fig. 3. Comparison of the high frequency regions of ^{1}H n.m.r. spectra of p(CPP–SA) 12.5:87.5 devices eroded for (a) 4 h; (b) 8 h; (c) 12 h; (d) 24 h; (e) 36 h; and (f) 48 h in pH 7.4 phosphate buffer USP.

Table 1
Combinations of peak integrals use to determine the dyad and end-group probabilities

Unit	Peak combination	Number of H nuclei
(CPP–CPP)	A	4
(SA–CPP)	B–F	2
(SA–SA)	(N/2)-D + F-K	4
(CPP*)	F	2
(SA*)	K	2
(SA–Ac + CPP–Ac)	L	3

(i) dyad sequence fractions, (SA-SA), (SA-CPP), (CPP-SA) and (CPP-CPP);
(ii) acetylated end-group fractions(SA-Ac) and (CPP-Ac);
(iii) carboxylic acid end group fractions, (SA*) and (CPP*).

The SA–CPP and CPP–SA dyad fractions are necessarily equal since the polymer chain direction cannot be specified. Henceforth, the notation (SA–CPP) is used to represent both dyads. The fractions of these structural elements were calculated from n.m.r. peak integrals weighted according to the number of contributing nuclei as listed in Table 1.

The number average degree of polymerization, *DP*, and the number average run lengths of SA and CPP sequences, $\tilde{n}_{SA}$ and $\tilde{n}_{CCP}$, were calculated from the following equations:

$$DP = \frac{2[(\mathrm{CPP}) + (\mathrm{SA})]}{(\mathrm{Ac}) + (\mathrm{SA}^*) + (\mathrm{CPP}^*)} \quad (1)$$

$$\tilde{n}_{SA} = \frac{2(\mathrm{SA})}{(\mathrm{Ac})(\mathrm{SA}) + (\mathrm{SA}^*) + (\mathrm{SA} - \mathrm{CPP})} \quad (2)$$

$$\tilde{n}_{CPP} = \frac{2(\mathrm{CPP})}{(\mathrm{Ac})(\mathrm{CPP}) + (\mathrm{CPP}^*) + (\mathrm{SA} - \mathrm{CPP})} \quad (3)$$

where

$$(\mathrm{Ac}) = (\mathrm{SA} - \mathrm{Ac}) + (\mathrm{CPP} - \mathrm{Ac})$$

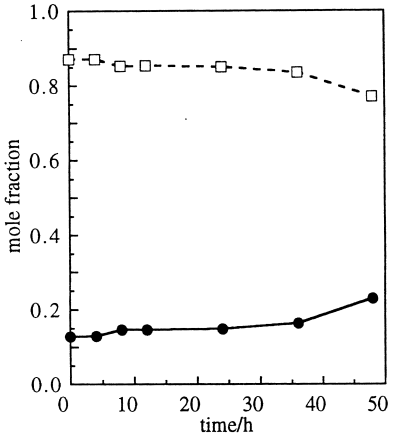

Fig. 4. Monomer fractions in p(CPP–SA) 12.5:87.5 devices during erosion in pH 7.4 phosphate buffer USP. □, (SA); ●, (CPP).

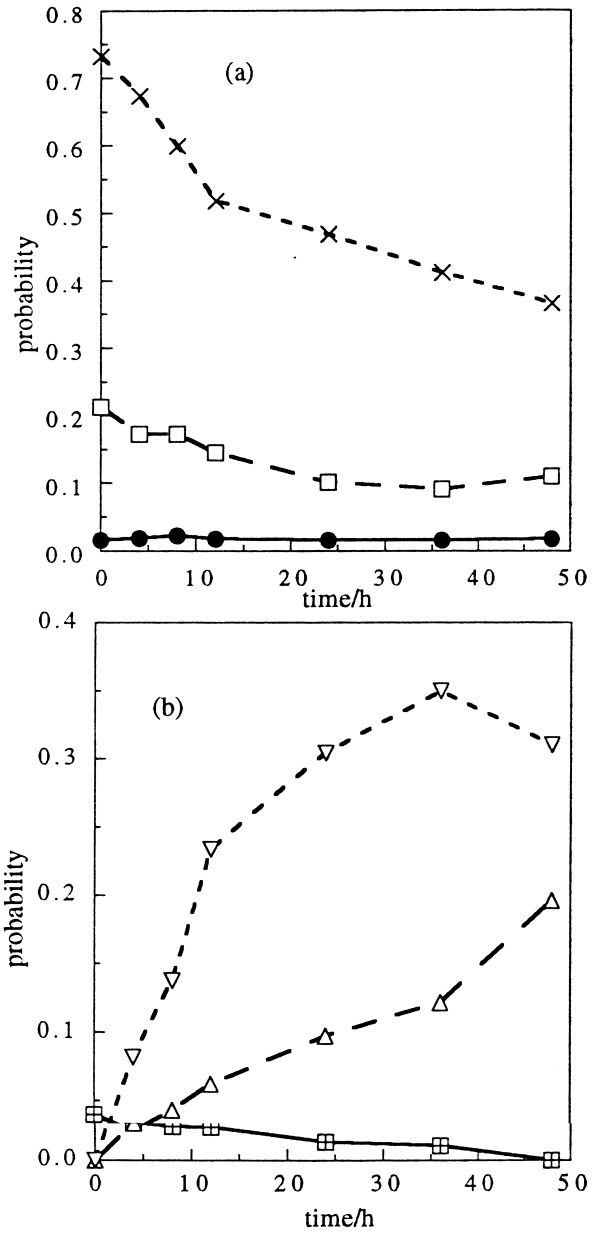

Fig. 5. Dyad and end-group fractions in p(CPP–SA) 12.5:87.5 devices during erosion in pH 7.4 phosphate buffer USP. (a) × , (SA–SA); □, (SA–CPP); ●, (CPP–CPP); (b) ▽, (SA*); △, (CPP*); ⊠ (SA–Ac + CPP–Ac).

It should be noted that in Eqs. (2) and (3), it has been assumed that the acetylated end-groups were divided between SA–Ac and CPP–Ac groups in the same proportion as the SA and CPP contents of the whole polymer. Fig. 4 shows the monomer fractions, Fig. 5 shows the dyad and end-group fractions, and Fig. 6 shows the number average degree of polymerization and sequence lengths as a function of erosion time for p(CPP–SA) 12.5:87.5 devices.

There were clear changes in polymer composition and sequence structure with erosion time. From the monomer fractions, it is apparent that devices became progressively richer in CPP overall as erosion proceeded. This finding is consistent with the results of previous studies [3,23] which

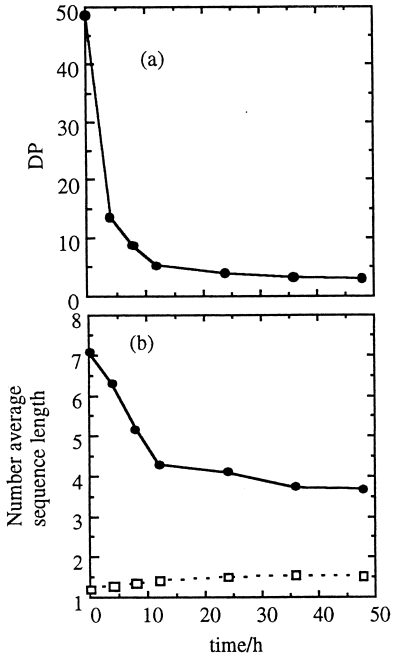

Fig. 6. Number-average sequence lengths in p(CPP–SA) 12.5:87.5 devices during erosion in pH 7.4 phosphate buffer USP. (a) *DP;* (b) ● $\tilde{n}_{SA}$; □ $\tilde{n}_{CPP}$.

have established that the dissolution rate of hydrolysed SA species is considerably faster than that of hydrolysed CPP moieties. Examination of the sequence distribution data provides a more detailed picture of the erosion process. The significant points are:

(i) (SA–SA) and (SA–CPP) decrease significantly, whereas (CPP–CPP) remains approximately constant.
(ii) (SA*) and (CPP*) increase significantly, whereas (SA–Ac) and (CPP–Ac) endgroups decrease essentially to zero.
(iii) *DP* and $\tilde{n}_{SA}$ decrease significantly whereas $\tilde{n}_{CPP}$ increases slightly.

The fact that little change is observed in (CPP–CPP) indicates the relatively low susceptibility to hydrolysis of the CPP–CPP link compared to SA–SA and SA–CPP links under the present conditions. The decrease in acetyl end-groups indicates the relatively high susceptibility of the SA–Ac and CPP–Ac links. The acetic acid formed by hydrolysis of the acetyl end-groups is presumably eluted into the aqueous medium.

Considering the SA* and CPP* end-groups, it should be noted that it is possible only to determine the proportion of SA or CPP carboxylic groups overall, and not whether these are polymer ends, oligomer ends, or SA or CPP monomers. The variation in (SA*) is in good agreement with the profiles of SA monomer content previously noted in other eroding p(CPP–SA) copolymers [6]. (CPP*) increases monotonically, whereas (SA*) increases rapidly between 0 and 12 h, reaches a maximum of ~35 mol% at 35 h, and thereafter decreases. Up to its maximum, (SA*) is approximately threefold greater than (CPP*), indicating that the rates of scission of SA–SA and SA–CPP links are approximately equal. Since the number of SA–SA links is approximately three times greater than the number of SA–CPP links, this implies that the rate constant for SA–CPP hydrolysis is some three-fold greater than that for SA–SA hydrolysis. A study [24] of the hydrolysis of acetic anhydride, benzoic anhydride and the mixed acetic/benzoic anhydride in 60:40 dioxane–water at 25°C gave rate constants of 6.6×10^{-5}, 0.22×10^{-5} and 4.85×10^{-5} s^{-1}, respectively. From these data, it might be expected that the rate constants for SA–SA and SA–CPP hydrolysis would be comparable. However, it should be borne in mind that in the solid devices, the SA–SA and SA–CPP units are not necessarily exposed equally to water.

Since limited dissolution of degradation species occurs during the early stages of polyanhydride erosion [23,25], the SA* content of the devices increases rapidly as hydrolysed SA units accumulate within the polymer. Size exclusion chromatography [25] indicated that at this stage the majority of SA* units originated from low molecular weight polymer chains–high oligomers. Between 12 and 36 h, despite continuing hydrolysis, there is a reduction in the rate of SA* accumulation within the eroding devices. This reduction, which is coincident with the onset of significant device weight loss (Fig. 1), may be explained by the preferential dissolution of hydrolysed SA species into the buffer. As chain scission continues, an increasing proportion of low molecular weight (hydrolysed) SA species are lost from the devices by dissolution, until eventually after 48 h erosion the rate of loss exceeds the rate of formation and consequently the SA* content of the devices starts to decline.

In contrast to SA*, the concentration of CPP* within the devices increased almost linearly during the initial 36 h of device erosion (Fig. 5b), evidence that throughout this phase the rate of CPP* formation exceeds the opposing CPP* depletion brought about by dissolution. Such behaviour is consistent with the findings of recent studies which have shown that SA* induced microenvironmental pH reductions and buffer saturation may suppress CPP* dissolution during the early stages of polyanhydride erosion [6]. Between 36–48 h there is an apparent increase in the rate of CPP* accumulation within the devices which was initially thought might be due to an increase in the rate of chain scission and/or a decrease in the rate of CPP* dissolution. However, neither of these explanations is supported by existing data. ^{1}H n.m.r. sequence length analysis (Fig. 6) and molecular weight measurements [25] indicate that there is no significant change in the rate of chain scission between 36-48 h. Also, monomer release profiles for p(CPP–SA) copolymers demonstrated that the rate of CPP* dissolution typically increases at this stage when the proportion of SA* within the device reaches its maximum and starts to decline [6].

3.4. Solid-State ^{1}H and ^{2}H n.m.r. spectroscopy

Fig. 7 shows spectra of the two uneroded polymers and

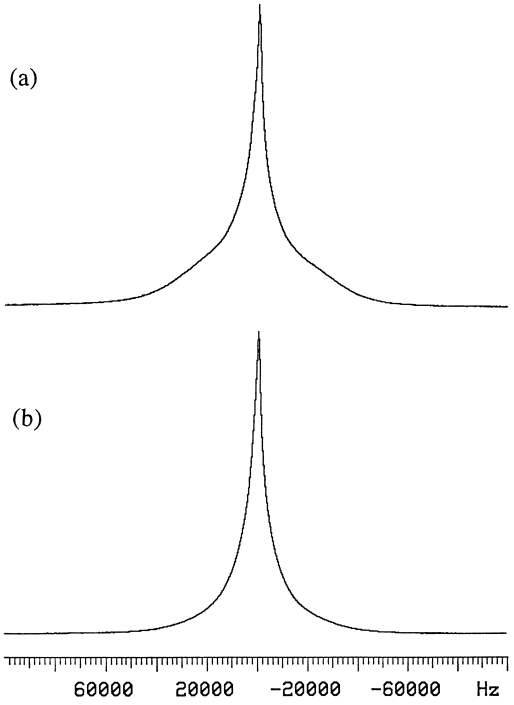

Fig. 7. Broadline ^{1}H n.m.r. spectra of p(CPP–SA) devices. (a) uneroded p(CPP–SA) 12.5:87.5; (b) uneroded p(CPP–SA) 30:70. The vertical scale of each spectrum have been individually adjusted so that each spectrum is the same plotted physical height.

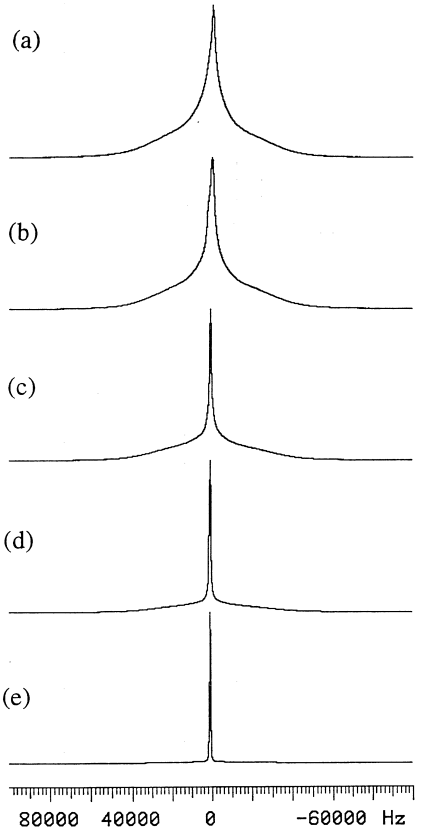

Fig. 8. Broadline ^{1}H n.m.r. spectra of p(CPP–SA) 12.5:87.5 as a function of erosion time. (a) uneroded; (b) 8 h; (c) 16 h; (d) 24 h; and (e) 48 h. The vertical scale of each spectrum was individually adjusted so that each spectrum is the same plotted physical height.

Fig. 8 shows spectra of p(CPP–SA) 12.5:87.5 as a function of erosion time.

All spectra clearly showed relatively broad and narrow components, the difference being particularly marked for samples eroded for more than 12 h. The components originate as a result of differences in the nuclear relaxation characteristics of distinct populations of protons present within the samples. The broad resonance line indicates the presence of large internuclear dipole–dipole interactions characteristic of species with highly restricted mobilities. In polymers, such rapidly relaxing nuclei (short transverse relaxation time, T_2) are typical of protons associated with a crystalline or glassy phase [13]. In contrast, molecular motion in a more mobile (rubbery) phase partially averages dipole–dipole interactions, giving a relatively narrow signal component (long T_2). In the uneroded polymers, it is apparent that the contribution of the broad component is more significant in p(CPP–SA) 12.5:87.5 than in p(CPP–SA) 30:70 since in the former, there is an obvious demarcation of the broad component defined by two points of inflection in the lineshape at $\sim \pm$ 20 kHz and the intensity perceptibly extends to $\sim \pm$ 45 kHz, while in the latter, the differentiation of the broad component is much less pronounced and its contribution to the total spectral area is considerably lower. The difference can be explained by the higher proportion of motionally constrained macromolecular protons present in p(CPP–SA) 12.5:87.5 resulting from the higher crystallinity of this material [26].

Close examination of the narrow resonance signal reveals subtle changes in lineshape during polymer erosion. Fig. 9 compares the central 10 kHz region of the broadline ^{1}H n.m.r. spectra of solid discs of p(CPP–SA) 12.5:87.5 corresponding to the narrow component at various times during polymer erosion.

The frequency zero has been arbitrarily set at the point of maximum intensity in the 48 h spectrum and the spectra have been plotted in absolute intensity mode in which the plotted intensity is proportional to the n.m.r. input signal provided the intensity factor is kept constant. Note that the intensity factor was lower by a factor of five for the spectra recorded after 20 h or more erosion. Although it is recognized that in n.m.r. it is difficult to compare the intensities of different samples, these spectra were recorded within a short period of time using identical instrumental conditions and (as close as practical) identical sample sizes; intensities were therefore comparable certainly within a factor of two. The most prominent change in the spectra is the increase in the relative intensity of the signal at $\sim$0–500 Hz by more than a factor of five over the period of erosion. The increase, which is particularly marked between 12 and 48 h, coincided with the phase of rapid water penetration observed by gravimetry (Fig. 1), suggesting that this signal is associated with relatively mobile

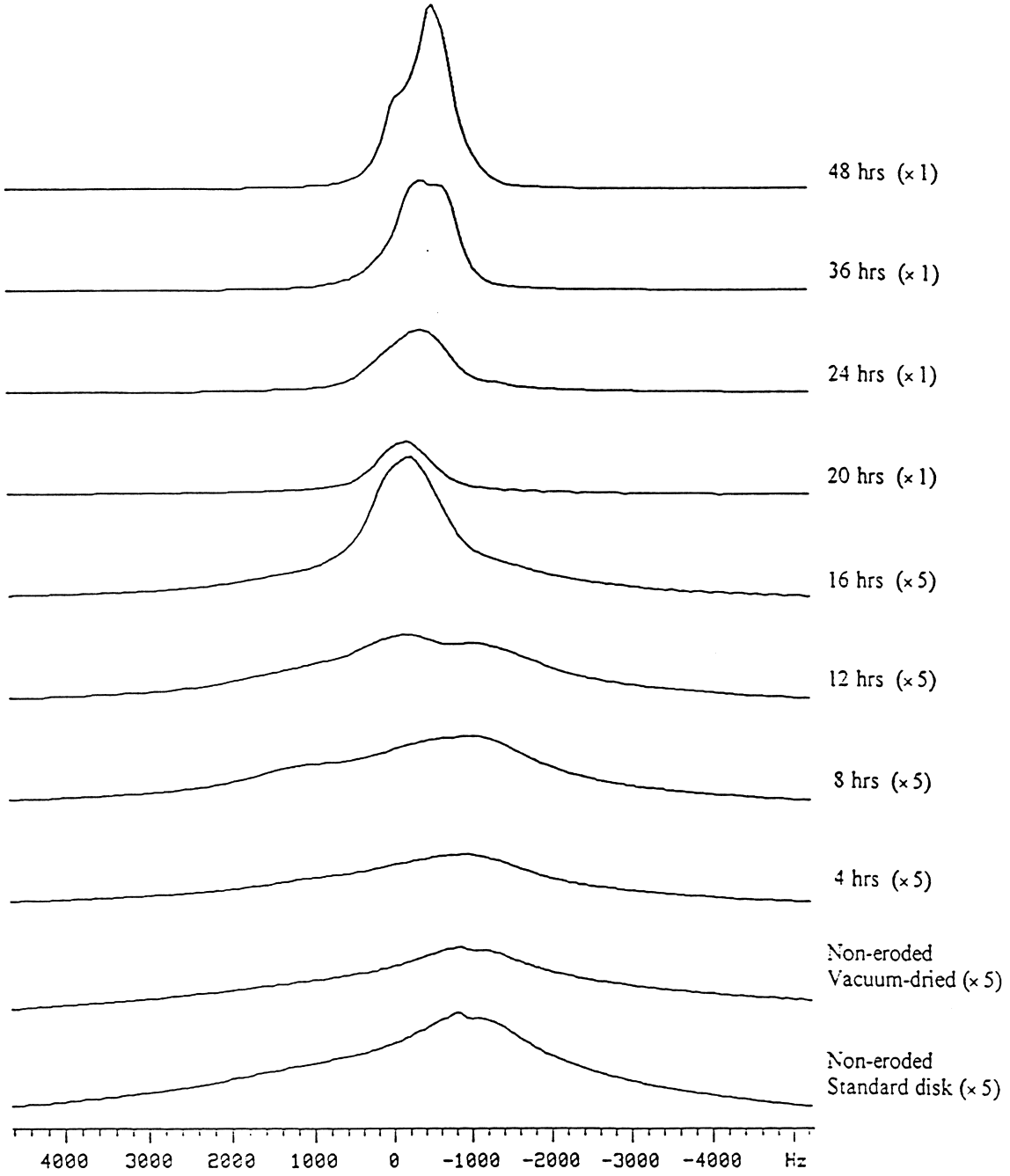

Fig. 9. Comparison of the central 10 kHz region of solid-state ^{1}H n.m.r. spectra of p(CPP–SA) 12.5:87.5 during erosion in pH 7.4 phosphate buffer USP. The spectra have been plotted in absolute intensity mode with an intensity factor lower by a factor of five at 20 h or greater.

absorbed water. However the linewidth of this signal is considerably larger than that of pure water (ca. 10 Hz on this instrument), presumably due to a decrease in the mobility of water protons when absorbed in the polymer, although the effects of cross-relaxation and proton exchange between water and the polymer [27], magnetic field inhomogeneities and paramagnetic impurities may also contribute. Similar results were obtained for p(CPP–SA) 30:70 (data not shown) although the spectral changes reflected the slower rate and extent of water absorption in this more hydrophobic polymer (Fig. 1).

The assignment of this narrow line to adsorbed water was confirmed by recording ^{2}H spectra of solid discs of p(CPP–SA) 12.5:87.5 eroded using deuteriated buffer; Fig. 10 shows ^{2}H spectra as a function of erosion time plotted in absolute intensity mode. As in the comparison of ^{1}H intensities in Fig. 9, the instrumental conditions and sample sizes were as identical as practical, and the ^{2}H intensities may be compared with better than a factor of two. All samples showed a narrow ^{2}H peak whose intensity increased by more than a factor of five over the erosion period.

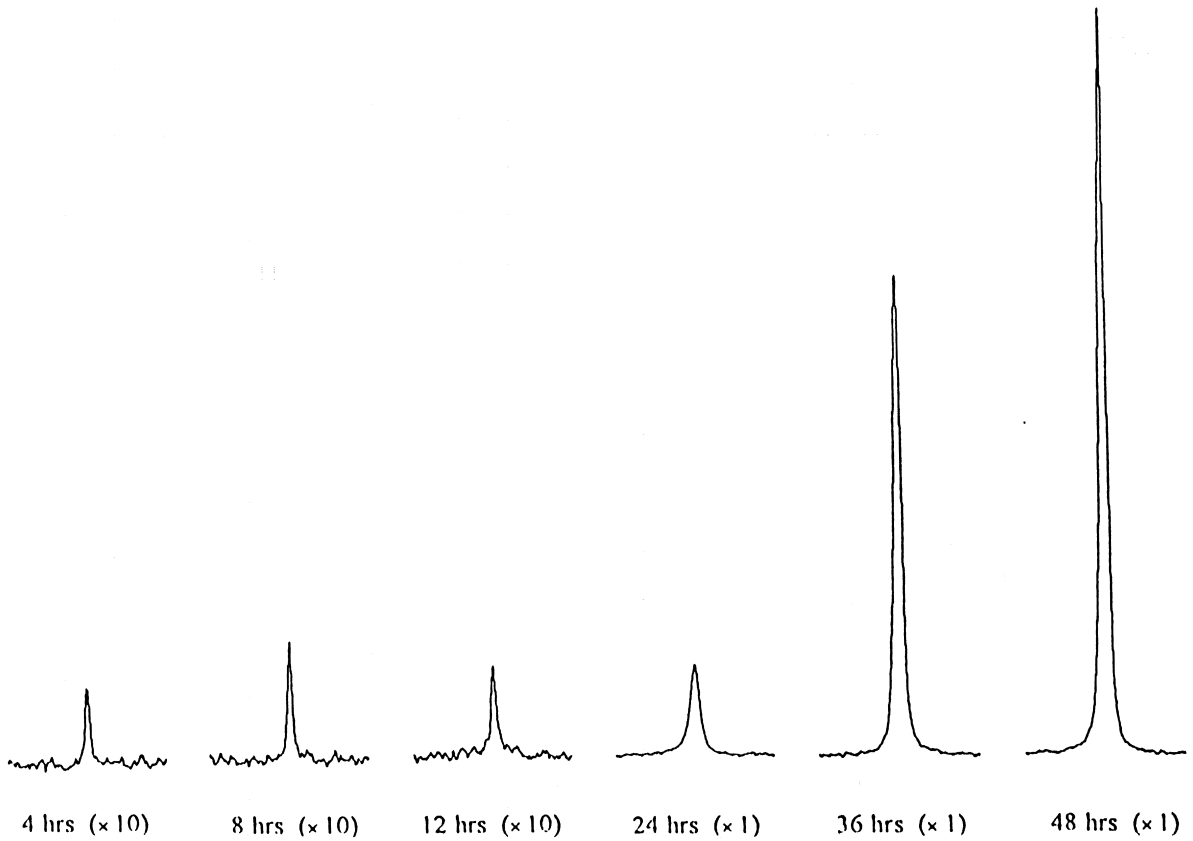

Fig. 10. ^{2}H n.m.r. spectra of solid p(CPP–SA) 12.5:87.5 eroded for various periods in deuterated pH 7.4 phosphate buffer USP. The width of each spectrum is 4 kHz. The spectra have been plotted in absolute intensity mode, the figures in parentheses denoting the relative intensity scaling.

Other fine structure was also apparent in the narrow ^{1}H resonance signal during the early stages of erosion. For p(CPP–SA) 12.5:87.5, within 8 h two signals were observed, one to low frequency at ca. -1.1 kHz and the other to high frequency at ca. +1.4 kHz (Fig. 9). Both signals remained resolved at 12 h erosion, but thereafter were obscured by the developing water peak. The approximate chemical shifts of the signals, calculated with reference to the water proton peak (assigned as 4.7 ppm [28]), were 1.9 and 7.9 ppm for the low frequency and high frequency signal, respectively. It is suggested that these resonances are attributable to mobile degradation products from chain hydrolysis, the 1.9 ppm signal from aliphatic protons originating from SA units and the 7.9 ppm signal from aromatic protons from CPP. Both assignments are consistent with the findings of the high resolution ^{1}H n.m.r. analysis of eroded devices reported earlier. In p(CPP–SA) 30:70, similar signals only became apparent after 12 h erosion but remained resolved until 24 h (data not shown), presumably due to slower erosion in this copolymer.

Further analysis of the broadline ^{1}H n.m.r. spectra was performed by component analysis. In accordance with criteria proposed by Kenwright and Say [11], spectra were analysed into the minimum number of components necessary to adequately represent the experimental lineshapes. In the case of 0-20 h eroded p(CPP–SA) 12.5:87.5 samples

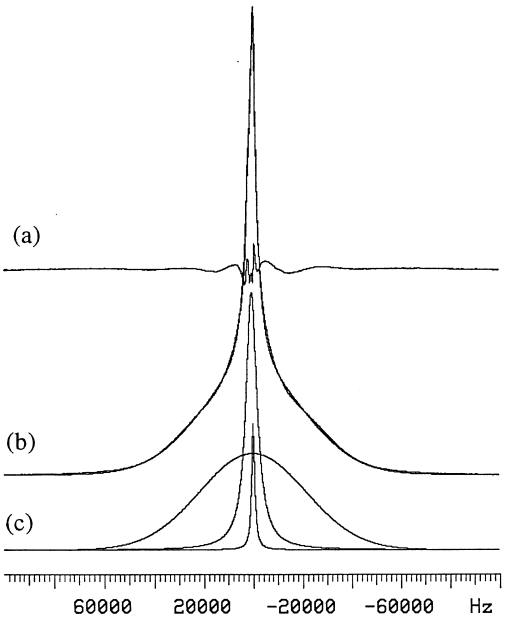

Fig. 11. Three-component analysis of the ^{1}H solid-state n.m.r. spectrum of p(CPP–SA) 12.5:87.5 after erosion in pH 7.4 phosphate buffer USP for 8 h. (a) residual signal from subtraction of the fitted and experimental lineshapes; (b) superposition of the experimental and fitted lineshapes; (c) broad, intermediate and narrow components.

Table 2
Linewidths of the components of the broadline ^{1}H n.m.r. spectrum of p(CPP–SA) 12.5:87.5 devices during erosion in pH 7.4 phosphate buffer USP

	Linewidth (kHz)					
	p(CPP–SA) 12.5:87.5			p(CPP–SA) 30:70		
Time (h)	Broad	Intermediate	Narrow	Broad	Intermediate	Narrow
0	52.0	9.3	1.9	41.6	12.0	2.5
4	52.3	8.9	2.4	44.0	15.1	3.0
8	50.8	5.4	1.5	44.5	16.2	3.1
12	52.5	16.0	3.5	43.4	13.5	2.9
16	51.6	7.1	1.0	43.7	21.1	3.4
20	52.6	13.0	0.8	44.0	21.6	3.0
24	50.3	-	0.9	41.0	6.0	1.1
36	61.3	-	0.8	38.9	-	0.9
48	79.4	-	0.6	39.4	-	0.8

and 0-24 h eroded p(CPP–SA) 30:70 samples, in addition to broad and narrow lineshape components, inclusion of a third intermediate component was necessary to achieve a satisfactory fit to the experimental data. A Gaussian lineshape was used for the broad component and a Lorentzian lineshape for the intermediate and narrow components. It is recognized that due to instrumental imperfections in recording such broad lines, the component analysis should only be used semi-quantitatively as a guide to the nature of any morphological changes. The outcome of a typical three component analysis is illustrated in Fig. 11. Linewidths are given in Table 2, and relative intensities (integrals) are plotted in Fig. 12.

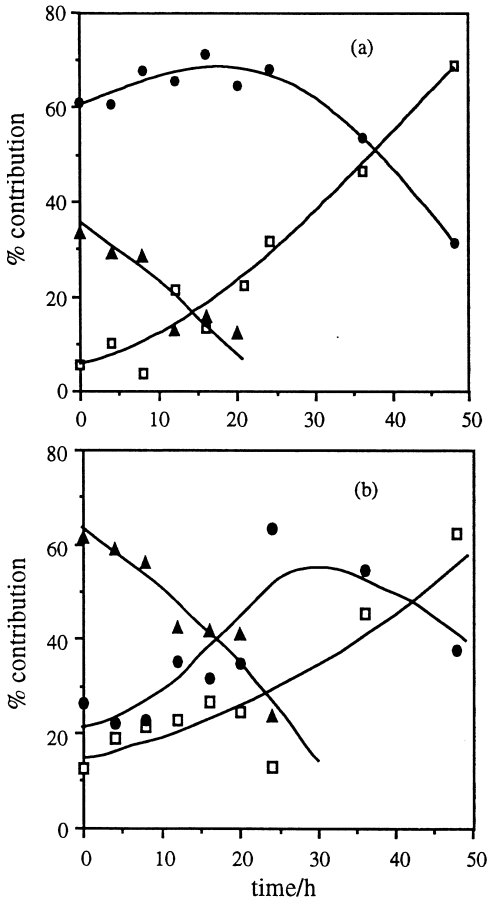

Fig. 12. Component relative intensities in the solid-state ^{1}H n.m.r. spectra of: (a) p(CPP–SA) 12.5:87.5; and (b) p(CPP–SA) 30:70 devices eroded in pH 7.4 phosphate buffer USP. ●, broad component; ▲, intermediate component; □, narrow component. The lines are for guidance only.

These results indicate that significant morphological changes accompanied the chemical changes described earlier. It is apparent that during erosion there was an appreciable increase in the narrow component intensity consisteny with the absorption of water as evidenced by the gravimetry results in Fig. 1 and by ^{2}H n.m.r. spectra (see above). Increased narrow signal contributions also arise due to an increase in the number of hydrolysed SA* and CPP* groups. However, the extent of such contributions is insufficient to account for the magnitude of the changes observed particularly during the early stages of erosion. For example at 4 h, the proton contribution of water and polymer end groups, calculated from gravimetric and SEC data, amounts to ~4% compared with the experimental value for the narrow component of ~10%. The additional narrow signal contribution probably originates from more mobile amorphous polymer protons, initially contributors to the intermediate and broad signal in the uneroded polymer, whose mobility has increased as a result of the erosion process. Such behaviour is consistent with the initial pattern of water absorption in other hydrophobic polymers; whereby water is absorbed near polar groups in the amorphous regions of the partially crystalline polymer [29].

During the first 24 h of erosion, the contribution of the broad component increased while the intermediate component decreased. These changes may be associated with an increase in polymer crystallinity, as noted during the first stage in the degradation of p(SA) [4,6], poly(glycolic acid) [29], poly(hydroxybutyrate-*co*-hydroxyvalerate) [30,31], and poly(β-propio-lactone) [32]. Crystallinity is thought to increase initially as a result of preferential hydrolytic attack on the amorphous regions of the polymer, because of their higher permeability compared with the crystalline phase. The preferential loss of amorphous material has been

confirmed in surface etched p(SA) using in situ atomic force microscopy [4]. Chu has also suggested that erosion may increase polymer crystallinity by yielding partially hydrolysed chain fragments whose reduced degree of entanglement enables them to realign themselves into a more ordered crystalline state [29]. This conclusion contradicts Göpferich and Langer [6] who reported that the crystallinity of p(CPP–SA) copolymers decreased during erosion. Here polymer crystallinity was estimated from the ratio of the enthalpies of fusion of the eroded polymer and the intact polymer crystallites. Unfortunately, these workers did not correct the experimental enthalpies for changes in the mass of the polymer during erosion. The enthalpies of fusion obtained were not representative of unit mass of polymer and therefore do not to provide a reliable estimate of polymer crystallinity.

Acknowledgements

The authors thank Dr. Avi Domb and Steve Gianos for their advice on polyanhydride synthesis, and John Friend and Shahireh Sadegholnjat for their assistance in conducting the n.m.r. experiments. This work was supported by a grant awarded to DLM by the BBSRC.

References

[1] Langer R. Ann Biomed Engng 1995;23:101.
[2] Mathiowitz E, Jacob J, Pekarek K, Chickering D. Macromolecules 1993;26:6756.
[3] Tamada JA, Langer R. Proc Natl Acad Sci 1993;90:552.
[4] Shakesheff KM, Davies MC, Domb A, Jackson DE, Roberts CJ, Tendler SJB, Williams PM. Macromolecules 1995;28:1108.
[5] Mäder K, Bacic G, Domb A, Swartz HM. Proc Int Symp Control Rel Bioact Mater 1995;22:780.
[6] Göpferich A, Langer R. J Polym Sci, Part A: Polym Chem 1993;31:2445.
[7] Göpferich A. Biomaterials 1996;17:103.
[8] Ron E, Mathiowitz E, Mathiowitz G, Domb A, Langer R. Macromolecules 1991;24:2278.
[9] Domb AJ, Maniar M. J Polym Sci, Part A: Polym Chem 1993;31:1275.
[10] Davies MC, Tudor AM, Hendra PJ, Domb AJ, Langer R. Proc Int Symp Control Rel Bioact Mater 1990;17:236.
[11] Kenwright AM, Say BJ. In: Ibbett RN, editor. NMR spectroscopy of polymers, chap. 7. London: Blackie, 1993.
[12] McBrierty VJ. In: Booth C, Price C, editors. Comprehensive polymer science, vol. 1, chap. 19. Oxford: Pergamon Press, 1989.
[13] Dybowski C, Brandolini AJ. In: Spells SJ, editor. Characterization of solid polymers: new techniques, chap. 7. London: Chapman and Hall, 1994.
[14] Oksanen CA, Zografi G. Pharm Res 1993;10:791.
[15] Fushimi H, Ando I, Iijima T. Polymer 1991;32:241.
[16] Allen PEM, Bennett DJ, Williams DRG. Eur Polym J 1993;29:231.
[17] Quinn FX, Kampff E, Smyth G, McBrierty VJ. Macromolecules 1988;21:3191.
[18] McCall DW, Douglas DC, Blyler LL, Johnson GE, Jelinski LW, Bair HE. Macromolecules 1984;17:1644.
[19] Schmitt EA, Flanagan DR, Linhardt RJ. Macromolecules 1994;27:743.
[20] Domb AJ, Langer R. J Polym Sci, Part A: Polym Chem 1987;25:3373.
[21] D'Emanuele A, Kost J, Hill JL, Langer R. Macromolecules 1992;25:511.
[22] Domb A, Langer R. Macromolecules 1989;22:2117.
[23] D'Emanuele A, Tamada J, Hill J, Domb A, Langer R. Pharm Res 1992;9:1279.
[24] Burton CA, Fuller NA, Perry SG, Shiner VG. J Chem Soc 1963:2919.
[25] McCann DL. Ph.D. thesis, University of Manchester, Manchester, 1997.
[26] Mathiowitz E, Domb A, Ron E, Mathiowitz G, Amato C, Langer R. Macromolecules 1990;23:3212.
[27] Schmidt SJ. In: Finley JW, Schmidt SJ, Serianni AS, editors. NMR applications in biopolymers. New York: Plenum Press, 1990.
[28] Abraham RJ, Fisher J, Loftus P. Introduction to NMR spectroscopy. Chichester: Wiley, 1988.
[29] Chu CC. J Appl Polym Sci 1981;26:1727.
[30] Holland SJ, Jolly AM, Yasin M, Tighe BJ. Biomaterials 1987;8:289.
[31] Satoh H, Yoshie N, Inoue Y. Polymer 1994;35:286.
[32] Albertsson AC, Lundmark S. Brit Polym J 1990;23:205.